Real time monitoring of interactions of gold nanoparticles with supported phospholipid lipid layers

Yousillya Bunga, Ritu Kataky

PII: S1572-6657(20)30529-4

DOI: https://doi.org/10.1016/j.jelechem.2020.114302

Reference: JEAC 114302

To appear in: *Journal of Electroanalytical Chemistry*

Received date: 28 December 2019

Revised date: 22 April 2020

Accepted date: 24 May 2020

Please cite this article as: Y. Bunga and R. Kataky, Real time monitoring of interactions of gold nanoparticles with supported phospholipid lipid layers, *Journal of Electroanalytical Chemistry* (2020), https://doi.org/10.1016/j.jelechem.2020.114302

Real time monitoring of interactions of gold nanoparticles with supported phospholipid lipid layers

Yousillya Bunga and Ritu Kataky* ritu.kataky@durham.ac.uk
Department of Chemistry, University of Durham, Lower Mountjoy, Durham, DH1 3LE, UK
*Corresponding author.

Abstract

Rapid methods for assessing engineered nanoparticle (NP) and their interactions with lipid membranes is important to several fields including pharmaceutical, clinical and toxicological studies. This study presents Resonance Enhanced Surface Impedance spectroscopy (RESI) as a method for real time assessment of NP interactions. RESI, used in a flow-injection analysis mode, provides a rapid and versatile method for revealing lipid disruption and reorganisation. Ferrocenated gold NPs (FcHT-AuNP) of three different sizes, were used to study their interactions with supported lipid layers. Electrochemistry and Atomic Force Microscopy (AFM) was used to complement RESI results, showing, that with increased incubation, AuNPs tend to agglomerate on the substrate. The effect of the change in hydrophilicity of the FcHT-AuNP upon oxidation, was immediately evident, using RESI, giving direct evidence that in its ferrocenium form the NPs tend to resist lipid adsorption.

Keywords

Phospholipids, gold nanoparticles, Resonance Enhanced Impedance spectroscopy, electrochemistry, real-time, Atomic Force Microscopy

1. Introduction

Modified gold nanoparticles (AuNPs) interactions with lipid bilayers are of fundamental importance in biomedical and biophysical studies. Factors such as the inherent large surface to volume ratio of NPs can be enhanced and harnessed by surface functionalisation, making NPs particularly tuneable to a wide range of functions, including biomedical and pharmaceutical applications [1,2,3,4,5]. However, the properties of AuNps that are engineered for interactions with cells need to be carefully monitored to avoid cytotoxic effects [6,7,8,9]

AuNPs interactions with cell membranes are dictated by the physicochemical properties of the NPs. Size and shape have been reported to have a significant influence on cellular uptake [9,10,11]. Roiter *et al,*[12] investigated the effect of silica NP sizes on lipid bilayers. Their studies revealed two distinct mechanism; one where the lipid bilayer envelopes polar NPs (> 22 nm) and the second, where polar

NPs formed pores in the lipid bilayer (< 22 nm). This effect was due to the curvature of the lipid membrane upon contact with the NPs, expressed as wrapping of the membrane around the NPs (fully or partially). Bailey and co –worker' investigations of citrate stabilised AuNPs of various sizes; 2, 5, 10 and 40 nm, and their interactions with lipid membrane revealed small losses of lipid mass (up to 6 ng) resulting in the removal of lipid molecules from the lipid bilayer [13]. The shape of the NPs also plays a crucial role in the cellular uptake of NPs, affecting the amount of time the NPs reside inside the cell and the length of time taken to get to the target cells [13,14]. Using similar particle sizes but different shapes, it was reported that spherical NPs penetrate cells more readily compared to rod-shaped NPs [9,15,16]

The surface charge and the balance of hydrophobic and hydrophilic groups of modified NPs are additional parameters influencing the translocation properties of AuNPs [6,17,18]. In general, cationic NPs can cause permanent destabilisation of the cell membrane via formation of pores in the membrane structure or membrane thinning whereas anionic and neutral NPs can penetrate the lipid membrane without causing major membrane disruption. [18,19]. Cationic NPs interact with negatively charged cell membranes via electrostatic attraction [20]. Coarse-grained molecular dynamics simulations have shown that cationic AuNPs interact with the phosphonate head group of the membrane made up of zwitterionic lipids altering of the tilt angle of the lipid molecules. Such interactions have been reported to perturb membrane architecture, without necessarily affecting the membrane fluidity [21,22,23] Another way that cationic NPs interact with lipid membrane is by the NPs becoming wrapped around by the lipid membrane, forming NPs-lipid vesicles. This interaction is driven by enhanced electrostatic attraction with the hydrophobic portion of the lipid bilayer resulting in membrane thinning, membrane rupture, and defect formation [24,25].

Interactions of NPs with cell membranes, resulting in internalization, can be either specific internalization, that requires the cell to actively interact with NPs into the cytoplasm, and non-specific internalization, in which random processes occur, where the cell has no active control. NPs modified with neutral ligands such as PEG (polyethylene glycol) [26,27], polysaccharides [28, 29], polymeric NPs [30], peptides and proteins [31] have been reported to facilitate the penetration of NPs as drug

carriers into the cell without signs of nonspecific NP-membrane interactions. Anionic NPs are shown to have non-specific cellular uptake pathways as reported by Ayala *et al.* [32], using carboxymethyl dextran-coated iron oxide NPs. Cationic NPs were reported to become engulfed within the lipid bilayer whereas anionic particles, are adsorbed at the surface of the membrane. Subsequently, absorbed, anionic NPs can form clusters at cationic sites on the plasma membrane [27,18,33]. Anionic NPs-membrane interactions, can, additionally, cause membrane gelation leading to the formation of lipid liposome· [34]. The various types of NP-Lipid membrane interactions possible are illustrated in ESI FigureS1.

Several experimental methods have been developed to probe AuNP interactions with surface supported cell membranes. Surface sensitive techniques such as Quartz Crystal microbalance with dissipation monitoring (QCM-D) [34,35,36,39], is a popular label-free and contact-free method for studying the interaction of NPs with model surfaces and supported lipid bilayers (SLBs). Vibrational sum frequency generation (SFG), [37,38] a second-order nonlinear optical spectroscopic method has been used to study NP/membrane interfaces showing that AuNPs surface area and surface functionalization affect the lipid bilayer flip-flop. Other methods include surface plasmon resonance (SPR) [39], total internal reflection fluorescence microscopy (TIRFM) [39], Atomic Force Microscopy, [40,41,42] and impedance spectroscopy [43]

The importance of a rapid method for investigations of NP and cell membrane interactions is crucial. In this work, Resonance Enhanced Surface Impedance (RESI) is presented as an alternative technique for a rapid assessment, in real time, for probing the effects of AuNPs with supported lipid membranes. Fundamental studies on size, incubation time and charge effects were performed using redox active ferrocene hexane thiol modified AuNPs (FcHTAuNP). AFM was used to study the effects of incubation time using non redox active, 1-dodecane thiol modified NPs (DDT-AuNP) .

The RESI methodology has been discussed in detail in previous publications. [44,45]. Briefly, Resonance enhanced surface impedance (RESI) is an electrochemical method using an instrument acquired from Layerlab AB z-LAB, Sweden, (ESI, Section 1, Figure S3) to effectively calculate real-time changes in capacitance and electrical resistance at surface interfaces. The instrument can perform

measurements at a user-defined temperature within the range of 20 and 40 ^{o} C (± 0.1 ^{o} C). RESI provides an efficient method for resolving small capacitance changes of less than 0.2 pF with a time resolution of 0.25 Hz. A surface process will prompt a change in interfacial capacitance and resistance, leading to a resonance peak shift. Surface adsorption processes decrease capacitance, whilst desorption processes cause a capacitance increase. Surface capacitance additionally responds to changes in dielectric properties, charge distribution, molecular organization and conformational changes.[44].

2.Experimental section

2.1 Chemicals Reagents and Solvents

1-dodecanethiol (DDT), 6-(Ferrocenyl) hexanethiol (FcHT), potassium phosphate monobasic (KH_2PO_4), potassium phosphate dibasic (K_2HPO_4), potassium nitrate (KNO_3), sodium perchlorate ($NaClO_4$), ethanol (EtOH) and toluene were purchased from Sigma-Aldrich. 1,2-dipalmitoyl-sn-glycero-3-phosphothioethanol (DPPTE), 2-oleoyl-1-palmityol-sn-glycero-3 phosphocholine (POPC) were purchase from INstruchemie, the Netherlands. Structures of molecules used for NP and substarte modification are shown in ESI Figure S3.

All solvents used were without purification and all solutions were made with purified (resistivity > 18.2 MΩ cm) water from a Sartorius Atrium Comfort I water purifying system.

2.2 Methods and Techniques

2.2.1 Synthesis and Functionalisation of AuNPs. 1-dodecanethiol (DDT, Sigma-Aldrich) stabilised AuNPs were synthesised using the Brust–Schiffrin method [46]. To obtain 6-(Ferrocenyl) hexanethiol modified NPs, a DDT-AuNPs colloid was mixed with an equal volume of 6-(Ferrocenyl) hexanethiol (FcHT, 10 mM, Sigma-Aldrich) in toluene, shaken on a vortex stirrer for 48 hours. The FHT-metal NPs were purified by sonication, followed by extraction of solvent and re-dispersion in ethanol

solvent for storage.

AuNPs were characterised using transmission electron microscopy (TEM; JEOL 2100F FEG TEM); TEM samples were prepared by air drying TEM grids made of copper mesh, pipetted with droplets of the colloid solutions. ImageJ software was used for particle size determination, measured with a minimum of 150 particles, ESI (Figure S4). Particle size distribution from TEM analyses demonstrated spherical shape for all samples with average core diameter sizes (5.5 ± 2.9 nm), these will be referred to as 5 nm FcHT-AuNPs; 11 ± 0.69 nm , these will be referred to as 10 nm FcHT-AuNPs; and 22 ± 2.9 nm , these will be referred to as 20 nm FcHT-AuNPs. DDT-AuNPs used for the AFM studies were 2.8 ± 1.0 nm

2.2.2 Preparation of organic lipid solutions. 1,2-dipalmitoyl-sn-glycero-3-phosphothioethanol (DPPTE, INstruchemie, the Netherlands), received in powder form, was dissolved in chloroform (Sigma-Aldrich), to form a 1mM solution which was then dried in a clean glass vial under N_2 stream, re-dissolved in 99.5% ethanol (1ml, Sigma-Aldrich) and stored in the fridge until use. 2-oleoyl-1-palmityol-sn-glycero-3-phosphocholine (POPC, Sigma-Aldrich), received as a lipid solution in chloroform, was dried in a clean glass vial under N_2 stream then the vial was left in a desiccator overnight to remove any remaining solvent. The dry lipid was rehydrated using phosphate buffer solution (PBS, 0.1 M, Sigma-Aldrich) making lipid concentration of 1 mg/ml. For POPC lipid vesicles to form, the solution was sonicated for 45 min. All lipid solutions were stored in the fridge until use.

2.2.3 Substrate modification. Substrates used for electrochemistry,z-lab and AFM measurements were cleaned in a 1:1:5 solution of hydrogen peroxide (25%), ammonia (30%) and Milli-Q water at 85 C for 10 min, rinsed with Milli-Q water, and then immersed in DPPTE in ethanol (99.5%) for 48 hours at 4 °C. Any loose thiols on the electrode surface were removed by rinsing with ethanol and water, creating the tether monolayer. The SAM modified electrodes were immersed in a solution of POPC lipid vesicles and the tBLM (tethered bilayer lipid membrane) layer was left to form overnight by vesicles fusion process for the AFM and electrochemistry measurements. t-BLM formation on the z-lab chips was monitored in real time as described in Section 3.1.

2.2.4 Atomic Force Microscopy. Atomic Force Microscopy was used to determine the morphological changes to the lipid membranes. The equipment used for all AFM measurements was Nanoscope V MultiMode 8 and NCR-50, AFM tapping mode was used throughout the experiments. The height images were analysed NanoScope Analysis 1.5.

Glass microscope slides were used as substrates in AFM experiments. These were chemically cleaned by immersion in different solutions then sonicated for 15 min at each step; acetone, propanol, a mixture of decon90 and deionised water (1:3 ratio) and deionised water. The substrates were then blow dried with pure N2. Gold substrates were prepared by evaporating 100 nm of gold thin film on a glass slide with 10 nm chromium layer for adhesion using an electron-beam (e-beam) evaporator.

2.2.5 Electrochemistry. Electrochemical measurements (Cyclic Voltammetry, Differential Pulse Voltammetry and Impedance measurements) were performed on Autolab PGSTAT 12 potentiostat (Metrohm Autolab B. V.) using NOVA 2.0 software for both measurements and data analysis. The measurements were performed in an electrochemical cell containing the electrolyte solution using three-electrode configuration; platinum wire as the pseudo reference electrode, a platinum flag as the counter electrode and the gold working electrode (WE) .The WE were purchased from BASi (West Layfette, US) with a WE area 0.02 cm^2. The WEs were polished with diamond polish slurries in a figure-eight pattern, and then sonicated with ethanol and water for 10 min, soaked in piranha solution (mixture of H_2SO_4 and H_2O_2 at 3:1 volume ratio) for 5 min followed by another sonication in water for 10 min then drying with N2 gas. Further cleaning was carried out in an electrochemical cell with cyclic voltammetry (CV) in 1.0 M H_2SO_4 between 0 and 1.4 V (vs. Ag/AgCl reference electrode) at a scan rate of 0.1 V/s until a stable voltammogram was obtained.

The procedure followed for electrochemical measurements for both BLM and SAM modified electrodes was

1. The modified electodes were incubated in FcHT-AuNP solutions.
2. The electrodes were then taken out of the solution and rinsed with MilliQ water
3. Electrochemical measurements were performed in background electrolyte using cyclic

voltammetry (CV) and differential pulse voltammetry (DPV)

Both CV and DPV techniques were used to follow the behaviour of redox active FcHPT-NPs on SAM and BLM modified electrodes. For the FcHT-AuNPs, an estimate of the amount of charge required for oxidation of the FcHT-AuNPs was calculated using $Q = \frac{A}{\upsilon}$ and, where Q is the amount of charge required for oxidation, A is the integrated area under the oxidation peak, ν is the scan rate (50 mV/s) (Table 1). However the CVs were obtained varied is shape and we did not use them for estimating surface coverage.

DPV is a more sensitive technique which can be adapted to an approximate estimation of surface concentrations of adsorbed redox active molecules when the concentrations of adsorbate are low.[47].

DPV measurements at stationary electrodes are affected by preceeding voltage steps. DPV of surface confined molecules can be complicated by a parallel combination of double layer capacitance and potential dependent faradaic pseudocapacitance in series with uncompenstated cell resistance. Non ideal behaviour can arise if the faradaic pseudocapcitance undergoes changes during the lifetime of the pulse. However, if the surface concentration of adsorbate is low enough any nonideality (represented by 'r' in equation 2) can be neglected, at a low scan rate. In order to obtain approximate surface coverage, we used the equation when faradiaic pseudocapacitance is much larger than double layer capacitancnc [47]

$$\Gamma_T = \frac{2RT\, i_p}{r i_p + \frac{n^2F^2\Delta E}{2RT\tau e}} \qquad (1)$$

Where ΔE=pulse amplitude, τ= the time after the pulse application when the current is measured, e=2.718, r~0, where r is the non-ideality term, Γ_T the total surface coverage of reactant,i_p the peak current, F the Faraday constant, R the gas constant and T the temperature.

2.2.6 Surface capacitance measurements were carried out using z-LAB-210-S2 (Layerlab, Sweden). Gold sensor chips provided by Layerlab AB were cleaned by UV-ozone explosion for 10 min followed by Milli-Q water rinse; all measurements were carried out using z-Measure software from

the same company [44,45]. (ESI Section 1). The gold electrodes, had a total area of 0.002 cm^2 per electrode and spaced by a 30 μm gap,

The RESI capacitance can be calculated from the maximum resonance frequency, at f_0, when the current is minimum, and the total impedance is at the maximum. Below f_0, the circuit is inductive and above f_0, the circuit is capacitive and dominated by the electrode impedance. For most ordinary electrolytes, the solution resistance (R_s) matches the inductor resistance R_L (R_s~R_L) [1]. From the circuitry (ESI, Figure S3), the electrode pair becomes the resonator and its resonance frequency is related, relatively accurately, to the RESI capacitance (C), according to Eq.1, valid for an ideal RCL-resonator.

$$f_0 = \frac{1}{2\pi\sqrt{LC_R}} \qquad (2)$$

Where f_0 = resonance frequency, L = inductance and C_R = RESI capacitance.

RESI, data acquisition can be performed in real time, which enables time-resolved measurements with enhanced sensitivity and improved signal resolution. When a nanoparticle passes through the cell, it can form reversible agglomeration or pass through the flow cell. The effective capacitance and resistance in the region between the electrodes will change, accordingly, resulting in a shift in the actual resonance frequency.

An interpretation of the RESI capacitance (C_R) is complex in a flow cell and needs further exploration. In a qualitative explanation, the RESI capacitance (C_R) can be viewed as influenced by the interface at an electrode-electrolyte interface comprised of the compact layer (C_L) with the inner and outer Helmholtz planes and the diffusion layer (D_L). The capacitance increases with decreasing separation between the electrode surface and plane of closest approach of ionic charges. When an adsorbed layer comprised of NPs is deposited on the electrode surface, the electrolyte will be partially shielded from the electrode, if the adsorbed layer is insulating or result in a rougher and larger surface area, if it's conducting. This can be described as a serial connection between a Helmholtz-type capacitor (C_{CL}) and the diffuse layer capacitance (C_{DL}) with the total capacitance (C_R) given by:

$$\frac{1}{C_R} = \frac{1}{C_{CL}} + \frac{1}{C_{DL}} \qquad (3)$$

Where C_R = RESI capacitance, C_{CL} = compact layer capacitance and C_{DL} = Diffuse layer capacitance.

At planar surfaces and high electrolyte concentrations, the compact layer capacitances (C_{CL}) tend to be significantly smaller than diffuse layer capacitances (C_{DL}) and dominate values C_R ($C_{CL} \sim C_R$). C_{CL} is nominally determined by $\varepsilon\varepsilon_0 A d^{-1}$, where ε is the dielectric constant of the medium, ε_0, the permittivity of free space, A the electrode area and d the distance that separates the electrolyte from the electrode. In microfluidic systems, C_{DL} can vary empirically with bulk properties such as electrolyte charge, concentration, dielectric constants of solvents, physical structure of microfluidic channels and flow rates

3. Results and Discussions

3.1 Formation of supported lipid layers

The lipid formation bilayers on gold electrodes was monitored using RESI (Figure 1) and with CV using potassium $Fe(CN)_6^{3-/4-}$ as probe for the electroanalytical measurements, CV showed that redox reaction is completely inhibited, indicating that the film formed is pinhole-free,(ESI Figure S6).

The formation of a good tethered lipid bilayer on a gold electrode surface can be monitored at each step of bi-layer formation using RESI. Initially the gold electrodes were modified with DPPTE to form a self-assembled monolayer, SAM, followed by lipid vesicles fusion. The lipid bilayer formation was monitored in real time with the z-LAB, recording the changes in RESI capacitance values over time (Figure 1). After 15 min equilibration time, with constant flow of phosphate buffer, the value for the RESI capacitance was around 1825 ± 200 μF cm^{-2}, Upon injection of POPC lipid solution (20 min duration) an initial dip in capacitance was observed due to the of presence of lipids in background phosphate buffer. The recorded changes in the capacitance values denoted the stages of lipid bilayer formation:

i. Adsorption of lipid vesicles on DPPTE-modified gold sensors observed as a slight increase in capacitance values from its initial value at the start of the injection

ii. Vesicles fusion: small decrease in capacitance that was found to remain stable for up to 50 min

iii. Lipid vesicles rupture and molecules rearrangement on surface, seen by the dramatic decrease in RESI capacitance to 110 nF (ca 94% decrease from initial capacitance)

iv. Bilayer formation seen as the RESI capacitance value remained steady for 20 min

After the bilayer was formed on the modified sensor, defects were checked by running a blank injection; only defects free sensors were used for this study to prevent penetration via pre-formed defects instead of penetration via NPs-membrane interactions. A further decrease in RESI capacitance values was recorded after the modified sensor was taken out of the system and flushed through with distilled water and re-fitted onto the zLAB, This decrease is attributed to the stabilisation of the membrane as any unerupted vesicles and loosely bound lipid fragments were washed out of the system.

3.2 Tethered SAMs and BLMs and interactions with FcHT-AuNPs

Tethered lipid layers (t-BLM) on solid supports retain their integrity by a combination of intermolecular forces between the lipid molecules which dictate their organisation, phase behaviour and stability. On exposure to a metallic particle, the t-BLM can interact locally with lipid domains by electrostatic interactions, lead to lipid restructuring by embedment, due to hydrophobic interactions or cause local deformation forming pores [48] Both the t-BLM and the NP have surface charges , enabling Derjaguin−Landau−Verwey−Overbeek (DLVO) ,electric-double layer interactions and van der Waals interactions [49].

In this work the interactions of AuNPs with SAMs and BLMs were studied as follows

i. the effect of increasing incubation time of modified electrodes in NP solutions using AFM for non-electroactive (dodecanethiolated) AuNPs, and electrochemical techniques for electroactive (ferrocenylthiolated) AuNPs.

ii. the effect of NPs sizes for electroactive (ferrocenylthiolated) gold NPs using their RESI and electrochemical responses.

3.2.1 Effect of incubation time of AuNPs on lipid membrane interactions

3.2.1.1 Electrochemical Measurements

BLM and SAM modified electrodes were exposed to FcHT-AuNP solutions (5 nm size, 2.8 μm concentration) to different times. The electrodes were then taken out of the solution and the NPs-phospholipid membrane interactions monitored using cyclic voltammetry (CV) (Figure 2). and differential pulse voltammetry (DPV) (ESI Figure S7, Table 1).

Redox activity was detected with the penetration of FcHT-AuNPs through both SAM and tBLM (not shown). A significant depletion in current density as well as a positive shift was observed for BLMs compared to SAMs. Further investigations were carried out with SAM modified electrodes (Figure 2 shows CVs, ESI Figure S7 shows DPVs). Initially, flat CVs were observed changing to well defined CVs after approximately 60m immersion in the FcHT-AuNP solution. Positive shifts in peak potential were recorded (Figure 2) from t = 60 to 480 min (0.06 V to 0.101 V) compared to a negative shift to -0.005 V at increasing incubation times. The approximate charge Q, the amount of charge required for oxidation, were estimated (Table 1). Calculations showed was an increase in the redox active charge shown by the increased *Q* values. for the first 120 min incubation duration. After 240 min, *Q* values decreased to 10.9 ± 3.5 μC cm^{-2} (t = 1800 min), this decrease in *Q* values was accompanied by a negative shift of the peak potential from +0.101 V to -0.005 V and a change in CV curves from peak-shaped to sigmoidal-shape (Figure2).

This is an interesting result that probably suggest the formation of agglomerated gold particles and of pin-holes. These initial results correspond with Atomic Force Microscopy AFM studies conducted with DDT-AuNPs discussed in the following section.

3.2.1.2 AFM measurements with DDT-AuNPs

Thin film microscope glass slides coated with Cr/Au thin film (10/100 nm, were used as substrates . The substrates were immersed in the lipid DPPTE solution for 48 hrs at 4 °C to form a lipid monolayer. The lipid modified gold substrates were then immersed in 1 ml of 1.2 μm DDT-AuNPs (size ~3nm) for different incubation times and analysed by atomic force microscopy (AFM), to allow the determination of changes to the morphology of the monolayer resulting from interaction with the AuNPs. (Figure 3).

AFM images (Figure 3) show a the progressive increase in the heights: from 3.62 ± 0.02 nm (t = 0) to 5.73 ± 0.51 nm (t = 60 min) to 7.31± 0.41 (t=480 min) suggesting that the NPs were embedded within the membrane creating defects in the lipid membrane. Similar results were recorded by Abraham *et al.* [50] with their AFM study on the penetration of cysteine coated AuNPs (10 nm) through DPPC monolayer (avg. length at 2 nm). They reported an increase in height to 7 nm. At t = 1920 min and a clear difference in peak height was seen, showing possible agglomeration of NPs, forming big NP clusters (width of 64 nm and height of up to 20 nm) with the presence of small shoulder peaks. These results and conclusion was supported by a study by Gordillo *et al.* [51] who reported that the main factor affecting the interaction of PEGylated AuNPs with phospholipid monolayer on mercury electrode was the NPs sizes; they observed that only small AuNPs (2-3 nm) were able to penetrate through the lipid monolayer compared to larger AuNPs (10 nm) that were adsorbed at the lipid's surface and, for longer immersion of the modified electrode in NPs solution, the smaller NPs formed a monolayer at the electrode's surface displacing the lipid membrane. More details on the AFM images and height profiles are available in ESI Figure S5

These AFM results support the electrochemical results showing that with increased incubation time, AuNPs penetrate and form agglomerates and defects. With the redox active FcHT-AuNPs, such agglomeration can result in electroactive islands with microelectrodes like behaviour, accounting for the sigmoidal shape of the CVs

3.2.2.1 Effect of size with FcHT-AuNPs

Reports have, shown that NPs sizes have a major impact on the NPs interaction with lipid membrane, with bigger NPs causing the removal of lipid molecules from the lipid bilayer architecture [52,53]. RESI and electrochemical techniques were used in this section to investigate the penetration behaviour and the electrochemical responses of FcHT-AuNPs, of different sizes, as they interact with lipid membranes.

3.2.2.2. RESI Studies

Real-time measurements were carried out by injecting 200 µl of FcHT-AuNPs solution (5, 10 and 20 nm) into the system fitted with tBLM-modified gold sensors. The background electrolyte solution was allowed to flow through the system for 15 min, till a stable response was obtained, NP suspensions and background solutions were injected, alternately, at regular intervals to check the structural integrity of the membrane layer.

Dips in RESI capacitance were observed as the FcHT-AuNP impacted the lipid surface. The RESI capacitance dips caused by the injections of 5 nm NPs , were attributed to the penetration of NPs through the lipid bilayer seen by a decrease of 63 % from initial RESI capacitance, when the background solution was flowing through the system (Figure 4; 5 nm). The U-shaped dip recovered showing that the NP was probably engulfed by the lipid layers. This was, followed by a recovery of the membrane integrity observed, as a return to background solution RESI capacitance values. A second injection showed a similar response.

Injection of 10 nm NPs showed a much smaller change of 5.9 nF in RESI capacitance, after the first injection (Figure 5;10 nm; point ‘c’). This can be attributed to the adsorption of NPs at electrolyte-lipid interface. Following the first injection of 10 nm NPs, the RESI capacitance did not return to the initial value, instead, small spiked responses were recorded. Sharp dips were evident following a second injection of 10 nm NPs, which we believe could be due to the removal of lipids by the NPs, from the bilayer. A study by Guo and co-workers [54] using a microfluidic device to monitor the translocation of hydrophobic AuNPs of different sizes, also reported that the penetration of larger NPs (>5 nm) through the bilayer caused lipid rupture as well as the removal of lipids from the bilayer as

these NPs are translocated. Similar phenomenon was replicated with the injections of 20 nm NPs, with lipid rupture occurring much earlier at about 60 m instead of 130 m compared to the 10 nm NPs

An important observation is that even with increased NP size, there is no drastic change to the RESI capacitance values, even after hole formation and lipid removal. It is likely that this type of phenomenon is attributable to the fluidic properties of lipid membrane enable self-recovery. [55]

3.2.2.3 Electrochemical Studies

Electrochemical studies were undertaken, looking at the responses of different sizes of FcHT-AuNPs and their penetration through tBLM modified gold macroelectrodes. tBLM modified electrodes were immersed in solutions of FcHT-AuNPs of three different sizes (5, 10 and 20 nm) for 60 min and electrochemical measurements (DPV) were carried out in background electrolyte solution after thorough rinsing.

In previous studies, small NPs (<5.5 nm AuNPs) were found to easily penetrate cells and localise inside nucleus of cell compared to larger ones (>16 nm AuNPs), which were found to be unable to enter the cells [57]. Our results are in accordance with these reports, as seen in the decrease in the magnitude of the current and surface coverage for the detection of FcHT-AuNPs at electrode's surface (Figure 5. and **Error! Reference source not found.**). The FcHT-AuNPs (5 nm) penetrated further into the lipid, enabling more NPs to penetrate through the lipid membrane, which are likely to aggregate at the electrode's surface, [57,58] consequently increasing their detected redox activity. The 5 nm FcHT-AuNPs penetration was attributed to the NP adsorption and further NPs embedment within the bilayer [59]. On the other hand, larger NPs (10 and 20 nm) have been reported to cause membrane thinning as well as defects formations i.e. nanoscopic pores/holes within the bilayer architecture.

Both electrochemical and RESI studies of the effect of size of NPs on lipid NP interactions is supported by previous studies. A study by Leroueil *et.al.*[60] suggested that small 2 nm NPs initially become adsorbed on the bilayer surface and eventually with more adsorption time, these formed

aggregates resulting in their penetration into the lipid structure via existing defects. However, larger 50 nm NPs were reported to induce lipid defects such as holes, membrane thinning as these NPs interacted with the lipid membrane.

3.2.3 Effect of potential control

Initial DPV measurements were performed to follow the effect of applying potential control to both SAM and tBLM modified electrodes. The electrodes were incubated with 5 nm FcHT-AuNPs in 0.1 M phosphate buffer for 60 m at -0.1V, rinsed thoroughly. DPV measurements taken in 0.2 M $NaClO_4$ (Figure ESI S8) by scanning in both the positive and negative directions. Sharp desorption peaks were observed at approximately +0.4 V in the reverse scan

The influence of applied voltage on t-BLM modified electrodes was studied with RESI measurements. The electrode potential was switched from open circuit potential to +0.4 V, which was chosen based on the potential at which desorption was observed in the DPV measurements. (Figure 6). The results generated, suggest that at positive potential hold, ferrocene moieties are partially oxidised to ferrocinium ions ,which are hydrophilic compared to ferrocene. It is likely that hydrophobic repulsions interactions result in a repulsion of FcHT-AuNps and a minimal perturbation of the lipid membrane architecture. In contrast at open circuit potentials a clear decrease in capacitance, was observed, indicating adsorption of the FcHI-AuNps.

4. Conclusions

Resonance enhanced surface impedance (RESI) technique is shown as a technique that is capable of rapid investigations of the effect of nanoparticles on biomimetic cell membranes. RESI results are supported by atomic force microscopy (AFM) and electrochemical techniques. Incubation time has a significant effect on the mechanism of NP penetration and recovery of NPs on lipid modified gold substrates showing different stages : NPs adsorption at lipid surface followed by lipid defects formation for eventually leading to lipid collapse and/or membrane displacement by NPs multilayers.

Both AFM and voltammetry results, showed formation of agglomerated NPs with increased incubation time.

NP size has a significant effect. Smaller NPs (< 5nm) , showed no effect in the destabilising the integrity of the membrane. Larger NPs (10 and 20 nm) were found to cause NPs adsorption at lipid-electrolyte interface and destabilisation of the membrane via the formation of lipid defects. However, despite lipid removal and hole formation caused by the larger NPs, RESI measurements suggest that lipid bilayer architecture is capable of self-recovery.

This work illustrates that RESI in an FIA configuration can provided a rapid and convenient method for investigation of NPs-membrane interaction for toxicological and pharmaceutical applications.

Acknowledgement

The authors would like to thank Engineering and Physical Sciences Research Council (EPSRC) for their funding support for the research

References:

1. D. Pissuwan, T. Niidome and M. B. Cortie, The forthcoming applications of gold nanoparticles in drug and gene delivery systems. J. Control. Release, (2011), 149, 65–71. https://doi.org/10.1016/j.jconrel.2009.12.006 ·
2. A. C. Templeton, W. P. Wuelfing and R. W. Murray, Monolayer-Protected Cluster Molecules Acc. Chem. Res., (2000), 33, 27–36. https://doi.org/10.1021/ar9602664
3. G. H. Woehrle, L. O. Brown and J. E. Hutchison, Thiol-Functionalized, 1.5-nm Gold Nanoparticles through Ligand Exchange Reactions: Scope and Mechanism of Ligand Exchange J. Am. Chem. Soc., (2005), 127, 2172–2183. https://doi.org/ 10.1021/ja0457718
4. T. L. Doane and C. Burda, The unique role of nanoparticles in nanomedicine: imaging, drug delivery and therapy, Chem. Soc. Rev, 41, 2885–2911. https://doi.org/10.1039/C2CS15260F2012
5. D. A. Giljohann, D. S. Seferos, W. L. Daniel, M. D. Massich, P. C. Patel and C. A. Mirkin, Gold Particles for Biology and Medicine., Angew. Chem. Int. Ed, (2010), **49**, 3280–3294. https://doi.org/10.1002/anie.200904359
6. T.S. Hauck, A.A. Ghazani, W.C. Chan, Assessing the Effect of Surface Chemistry on Gold Nanorod Uptake, Toxicity, and Gene Expression in Mammalian Cells. Small, (2008), 4, 153–159. https://doi.org/10.1038/srep11398
7. K.L. Aillon, Y. Xie, N. El-Gendy, C.J. Berkland, M.L. Forrest, M. L., Gold Nanoparticles Are Taken up by Human Cells but Do Not Cause Acute Cytotoxicity, (Small),3, 325– 327., https://doi.org/10.1002/smll.200400093
8. K.L. Aillon, Y. Xie, N. El-Gendy, C.J. Berkland, M.L. Forrest, M. L., Effects of Nanomaterial Physicochemical Properties on in Vivo Toxicity. Adv. Drug Delivery Rev., (2009), 61, 457–466. https://doi.org/10.1016/j.addr.2009.03.010
9. N. Lewinski, V. Colvin, R. Drezek, Cytotoxicity of Nanoparticles. Small., (2008), 4, 26–49. https://doi.org/10.1002/smll.200700595
10. B.D. Chithrani, A.A. Ghazani, W.C. Chan, Determining the Size and Shape Dependence of Gold Nanoparticle Uptake into Mammalian Cells. Nano Lett. (2006), 6, 662–668. https://doi.org/10.1021/nl052396o
11. S.-H. Park, S.-G. Oh, J.-Y. Mun and S.-S. Han, Loading of gold nanoparticles inside the DPPC bilayers of liposome and their effects on membrane fluidities., Colloids and Surfaces B: Biointerfaces, (2006) 48(2), 112-118. https://doi.org/10.1016/j.colsurfb.2006.01.006
12. Y. Roiter, M. Ornatska, A. R. Rammohan, J. Balakrishnan, D. R. Heine and S. Minko, Interaction of Nanoparticles with Lipid Membrane, Nano Lett., (2008), 8, 941–944, https://doi.org/10.1021/nl080080l
13. C. M. Bailey, E. Kamaloo, K. L. Waterman, K. F. Wang, R. Nagarajan and T.A Camesano, Size dependence of gold nanoparticle interactions with a supported lipid bilayer: A QCM-D study. Biophys. Chem., (2015), 203–204, 51–61. http://dx.doi.org/10.1016/j.bpc.2015.05.006
14. S. Salatin, S. Maleki Dizaj and A. Yari Khosroushahi, Effect of the surface modification, size, and shape on cellular uptake of nanoparticles., *Cell Biol. Int.*, (2015), 39, 881–890. https://doi.org/10.1002/cbin.10459
15. D. H. Kim, J. C. Park, G. E. Jeon, C. S. Kim and J. H. Seo, Effect of the size and shape of silver nanoparticles on bacterial growth and metabolism by monitoring optical density and fluorescence intensity., Biotechnol. Bioprocess Eng, (2017), 22, 210–217. https://doi.org/10.1007/s12257-016-0641-3
16. S. Dasgupta, T. Auth and G. Gompper, Nano Lett., Shape and Orientation Matter for the Cellular Uptake of Nonspherical Particles., (2014), 14, 687–693. https://doi.org/10.1021/nl403949h

17. A. Verma, O. Uzun, Y. Hu, Y. Hu, H.S. Han, N. Watson, S. Chen, D.J. Irvine, F. Stellacci, Surface-Structure Regulated Cell-Membrane Penetration by Monolayer Protected Nanoparticles. Nat. Mater. (2008), 7, 588–595. https://doi.org/101038/nmat2202
18. E.E Connor, J. Mwamuka, A. Gole, C.J. Murphy, M.D. Wyatt, E.C.Cho, J. Xie, P.A. Wurm,Y. Xia, Understanding the Role of Surface Charges in Cellular Adsorption versus Internalization by Selectively Removing Gold Nanoparticles on the Cell Surface with a I2/KI Etchant. Nano Lett. (2009), 9, 1080–1084. https://doi.org/10.1021/nl803487r
19. J. Lin, H. Zhang, Z. Chen and Y. Zheng, Penetration of Lipid Membranes by Gold Nanoparticles: Insights into Cellular Uptake, Cytotoxicity, and Their Relationship, *ACS Nano*, (2010), 4, 5421–5429. https://doi.org/10.1021/nn1010792
20. C. M. Goodman, C. D. McCusker, T. Yilmaz and V. M. Rotello, Toxicity of Gold Nanoparticles Functionalized with Cationic and Anionic Side Chains., Bioconjug. Chem.,(2004), 15, 897–900., https://doi.org/10.1021/bc049951i
21. A. Gupta, S. Mumtaz, C.-H. Li, I. Hussain and V. M. Rotello, Combatting antibiotic-resistant bacteria using nanomaterials., Chem. Soc. Rev., (2019), 48, 415–427., https://doi.org/10.1039/C7CS00748E
22. T. Tree-Udom, J. Seemork, K. Shigyou, T. Hamada, N. Sangphech, T. Palaga, N. Insin, P. Pan-In and S. Wanichwecharungruang, Shape Effect on Particle-Lipid Bilayer Membrane Association, Cellular Uptake, and Cytotoxicity., *ACS Appl. Mater. Interfaces*, (2015), 7, 23993–24000., https://doi.org/10.1021/acsami.5b06781
23. A. Velikonja, P. B. Santhosh, E. Gongadze, M. Kulkarni, K. Eleršič, Š. Perutkova, V. Kralj-Iglič, N. P. Ulrih and A. Iglič, Interaction between Dipolar Lipid Headgroups and Charged Nanoparticles Mediated by Water Dipoles and Ions., *Int. J. Mol. Sci.*,(2013) , 14, 15312–15329. https://doi.org/10.3390/ijms140815312.
24. Y. Li and N. Gu, Thermodynamics of Charged Nanoparticle Adsorption on Charge-Neutral Membranes: A Simulation Study., J. Phys. Chem. B, () 2010, 114, 2749–2754. https://doi.org/10.1021/jp904550b
25. V. V. Ginzburg and S. Balijepalli, Modeling the Thermodynamics of the Interaction of Nanoparticles with Cell Membranes., Nano *Lett.*, (2007), **7**, 3716–3722. https://doi.org/10.1021/nl072053l
26. P. B. Santhosh, S. Peni, J. Genova, A. Igli, V. Kralj-Igli and N. P. Ulrih, A study on the interaction of nanoparticles with lipid membranes and their influence on membrane fluidity., Journal of Physics: Conference Series 398 (2012) 012034., https://doi.org/10.1088/1742-6596/398/1/012034.
27. A. Verma and F. Stellacci, Effect of Surface Properties on Nanoparticle–Cell Interactions., Small, (2010), 6, 12–21. https://doi.org/10.1002/smll.200901158
28. G. Rossi and L. Monticelli, Simulating the interaction of lipid membranes with polymer and ligand-coated nanoparticles., Advances in Physics: X (2016) 1, 276-296., https://doi.org/10.1080/23746149.2016.1177468.
29. C. Lemarchand, R. Gref and P. Couvreur, Influence of polysaccharide coating on the interactions of nanoparticles with biological systems., Eur. J. Pharm. Biopharm., (2004), 58, 327–341. https://doi.org/10.1016/j.biomaterials.2005.04.041.
30. K. Yin Win and S.-S. Feng,. Effects of particle size and surface coating on cellular uptake of polymeric nanoparticles for oral delivery of anticancer drugs., Biomaterials. (2005), 26:2713–2722. https://doi.org 10.1016/j.biomaterials.2004.07.050.
31. M. Morishita and N. A. Peppas, Is the oral route possible for peptide and protein drug delivery?., Drug Discov. Today, (2006) , **11**, 905–910. https://doi.org/10.1016/j.drudis.2006.08.005
32. V.Ayala, A. P. Herrera, M. Latorre-Esteves, M. Torres-Lugo and C. Rinaldi, Effect of surface charge on the colloidal stability and in vitro uptake of carboxymethyl dextran-coated

iron oxide nanoparticles., J. Nanoparticle Res., (2013), 15, 1874. https://doi.org/ 10.1007/s11051-013-1874-0.

33. C. Wilhelm, F. Gazeau, J. Roger, J. N. Pons and J. C. Bacri, Interaction of Anionic Superparamagnetic Nanoparticles with Cells: Kinetic Analyses of Membrane Adsorption and Subsequent Internalization., Langmuir, (2002), 18, 8148–8155. https://doi.org/10.1021/la0257337
34. B. Wang, L. Zhang, S. C. Bae and S. Granick, Nanoparticle-induced surface reconstruction of phospholipid membranes., Proc. Natl. Acad. Sci. U. S. A., (2008), 105, 18171–18175. https://doi.org/ 10.1073/pnas.0807296105
35. C. A, Keller, B. Kasemo, Surface specific kinetics of lipid vesicle adsorption measured with a quartz crystal microbalance., Biophys J. (1998) Sep; 75(3): 1397–1402. https://doi.org/10.1016/S0006-3495(98)74057-3.
36. X.F. Zhang, S.H. Yang., Nonspecific Adsorption of Charged Quantum Dots on Supported Zwitterionic Lipid Bilayers: Real-Time Monitoring by Quartz Crystal Microbalance with Dissipation, Langmuir 2011, 27 (6), 2528−2535. https://doi.org/10.1021/la104449y
37. P. Hu, W. Qian, B. Liu, C. Pichan, Z. Chen Molecular Interactions Between Silver Nanoparticles and Model Cell Membranes, J. Phys. Chem. C 120 (2016) 22718–22729. https://doi.org/10.1007/s11244-018-0926-1
38. P. Hu, X. Zhang, C. Zhang, Z. Chen, Molecular interactions between gold nanoparticles and model cell membranes, Phys. Chem. Chem. Phys. 17 (2015), 9873–9884. https://doi.org /10.1039/C5CP00477B
39. P.-Å., Ohlsson, T. Tja¨rnhage, E. Herbai, S. Lo¨fås, and G. Puu, Liposome and proteoliposome fusion onto solid substrates, studied using atomic force microscopy, quartz crystal microbalance and surface plasmon resonance. Biological activities of incorporated components., Bioelectroch Bioenerg. (1995), 38:137–148
40. E. Kalb, S. Frey, and L. K. Tamm., Tethered Polymer-Supported Planar Lipid Bilayers for Reconstitution of Integral Membrane Proteins: Silane-Polyethyleneglycol-Lipid as a Cushion and Covalent Linker., *Biochim. Biophys. Acta*. (1992), 1103:307–316. https://doi.org/10.1016/S0006-3495(00)76391-0
41. Y. Roiter, M. Ornatska, A.R. Rammohan, J. Balakrishnan, D.R. Heine, S. Minko, Interaction of Nanoparticles with Lipid Membrane, Nano Lett. (2008), 8 (3), 941−944. https://doi.org/10.1021/nl080080l
42. T, A, Spurlin, A.A.; Gewirth, Effect of C60 on solid supported lipid bilayers., Nano Lett. (2007), 7 (2), 531−535. https://doi.org/10.1021/nl0622707
43. Y. Liu, Z. Zhang, Q, Zhang, G.L.Baker, R.W.Worden., Biomembrane disruption by silica-core nanoparticles: effect of surface functional group measured using a tethered bilayer lipid membrane., Biochim Biophys Acta. (2014) Jan; 1838(1), https://doi.org/1010.1016/j.bbamem.2013.09.007.
44. A. Lundgren, J. Hedlund, O. Andersson, M. Brändén, A. Kunze, H. Elwing, F. Höök, . Resonance-Mode Electrochemical Impedance Measurements of Silicon Dioxide Supported Lipid Bilayer Formation and Ion Channel Mediated Charge Transport., Anal. Chem. 83 (2011) 7800–7806. https://doi.org/10.1021/ac201273t.
45. Y.Bunga, R.Kataky, Silver nanoparticle impacts on gold electrode surfaces in flow-injection configuration., Sensors & Actuators B. Chemical, 290 (2019)140-146. https://doi.org/10.1016/j.snb.2019.03.065
46. R. L. Stiles, R. Balasubramanian, S. W. Feldberg and R. W. Murray, Anion-Induced Adsorption of Ferrocenated Nanoparticles., J. Am. Chem. Soc., (2008), 130, 1856–1865. https://doi.org/10.1021/ja074161f
47. A.P.Brown, F.C.Anson, Cyclic and Differential Pulse Voltammetric Behavior of

Reactants Confined to the Electrode Surface., Analytical Chemistry., (1977). 49, 11, 1589-1595.

48. K.L. Chen and G.D. Bothun, Nanoparticles Meet Cell Membranes: Probing Nonspecific Interactions using Model Membranes., Environ. Sci. Technol. (2014), 48, 873−880. https://doi.org/10.1021/es403864v.
49. X.Xiao, G.A. Montano, T.L. Edwards, A. Allen, K.E. Achyuthan, R. Polsky, D.R. Wheeler, S.M. Brozik. Surface charge dependent nanoparticle disruption and deposition of lipid bilayer assemblies. Langmuir (2012), 28 (50), 17396−17403. https://doi.org/10.1021/la303300b
50. N. Ábrahám, E. Csapó, G. Bohus and I. Dékány, Interaction of biofunctionalized gold nanoparticles with model phospholipid membranes., Colloid Polym. Sci., (2014), 292, 2715–2725. https://doi.org/10.1007/s00396-014-3302-0
51. G. J. Gordillo, Ž. Krpetić and M. Brust, Interactions of Gold Nanoparticles with a Phospholipid Monolayer Membrane on Mercury., ACS Nano, (2014), 8, 6074–6080. https://doi.org/10.1021/nn501395e
52. C. M. Bailey, E. Kamaloo, K. L. Waterman, K. F. Wang, R. Nagarajan and T. A. Camesano, Size dependence of gold nanoparticle interactions with a supported lipid bilayer: A QCM-D study., Biophys. Chem., (2015), 203–204, 51–61. https://doi.org/10.1016/j.bpc.2015.05.006
53. S.H. Park, S.G. Oh, J.Y. Mun and S.S. Han, Loading of gold nanoparticles inside the DPPC bilayers of liposome and their effects on membrane fluidities., Colloids Surf. B Biointerfaces, (2006), 48, 112–118. https://doi.org/10.1016/j.colsurfb.2006.01.006.
54. Y. Guo, E. Terazzi, R. Seemann, J. B. Fleury and V. A. Baulin, Direct proof of spontaneous translocation of lipid-covered hydrophobic nanoparticles through a phospholipid bilayer., Sci Adv. (2016) Nov 2;2(11):e1600261. https://doi.org/10.1126/sciadv.1600261
55. R. P. Carney, Y. Astier, T. M. Carney, K. Voïtchovsky, P. H. Jacob Silva and F. Stellacci, Electrical Method to Quantify Nanoparticle Interaction with Lipid Bilayers., ACS Nano, (2013), 7, 932–942. https://doi.org/10.1021/nn3036304
56. L. Shang, K. Nienhaus and G. U. Nienhaus, Engineered nanoparticles interacting with cells: size matters., J. Nanobiotechnology, (2014), 12, 5. https://doi.org/10.1186/1477-3155-12-5
57. S. Salatin, S. Maleki Dizaj and A. Yari Khosroushahi, Effect of the surface modification, size, and shape on cellular uptake of nanoparticles, Cell Biol. Int., (2015), 39, 881–890. https://doi.org/10.1002/cbin.10459
58. A. E. Nel, L. Mädler, D. Velegol, T. Xia, E. M. V Hoek, P. Somasundaran, F. Klaessig, V. Castranova and M. Thompson, Understanding biophysicochemical interactions at the nano–bio interface., Nat. Mater., (2009), 8, 543. https://doi.org/10.1038/nmat2442
59. Y. Liu and R. Mark Worden, Size dependent disruption of tethered lipid bilayers by functionalized polystyrene nanoparticles., Biochim. Biophys. Acta, (2015), 1848, 67–75. https://doi.org/10.1016/j.bbamem.2014.09.014.
60. P. R. Leroueil, S. A. Berry, K. Duthie, G. Han, V. M. Rotello, D. Q. McNerny, Baker James R., B. G. Orr and M. M. Banaszak Holl, Wide Varieties of Cationic Nanoparticles Induce Defects in Supported Lipid Bilayers., Nano Lett.,(2008), 8, 420–424., https://doi.org/10.1021/nl0722929

Figures and Tables

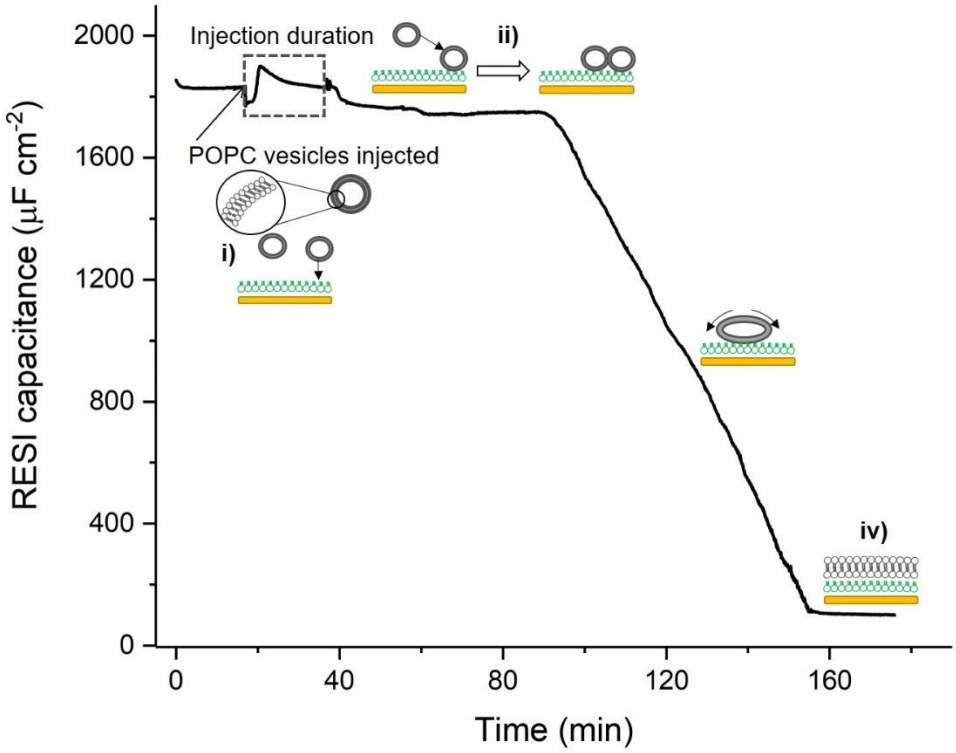

Figure1: Real time formation of lipid bilayer on SAM electrode chip; i) adsorption of lipid vesicles onto DPPTE-Au electrodes, ii) vesicle fusion, iii) lipid vesicle rupture and molecules rearrangement on modified sensor and iv) lipid bilayer or multilayers formed. POPC vesicle solution injected after 15 min system stabilisation with constant flow of 0.1 M PBS at fixed flow rate of 5 µL/min

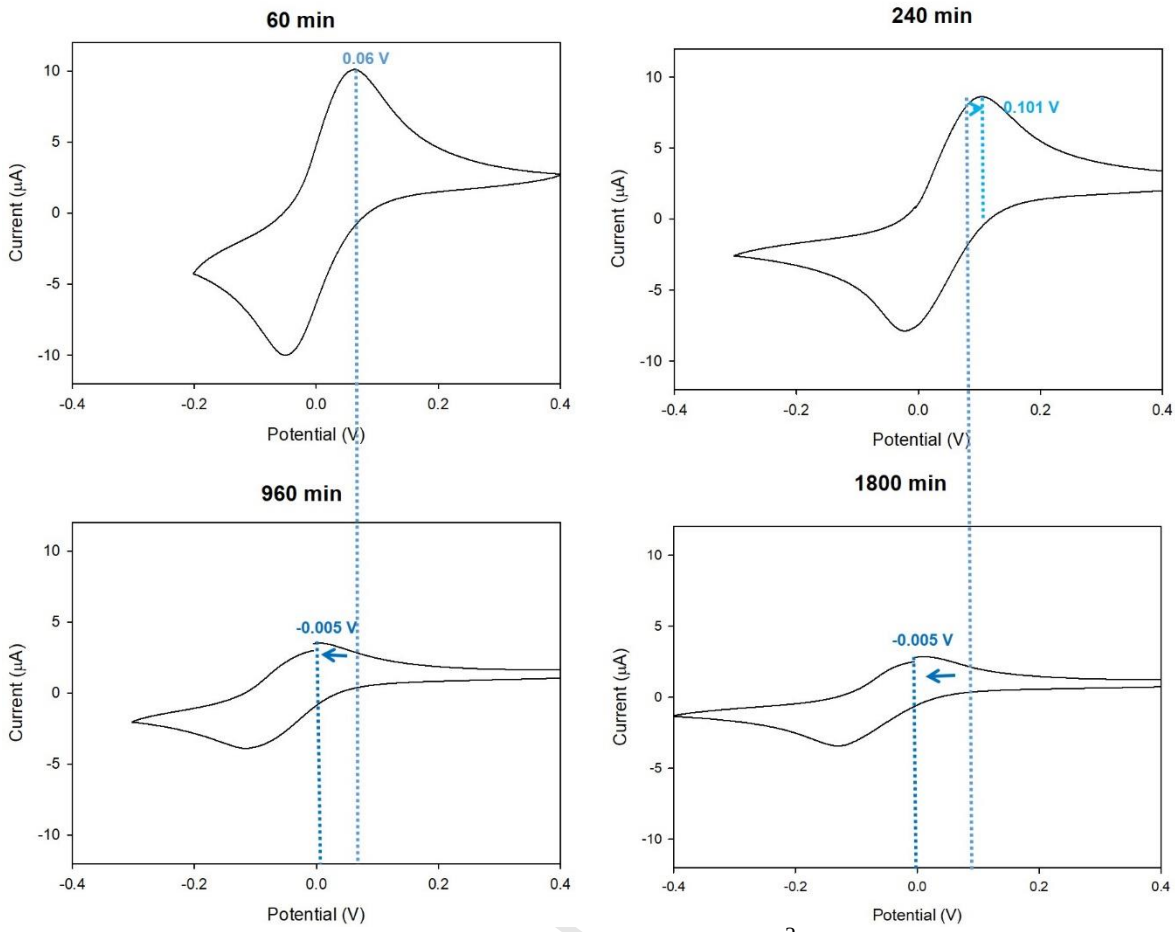

Figure 2: CVs of the SAM-modified gold electrode (0.02 cm^2) in 0.1 M KNO3 at 60, 240, 960 and 1800 min immersion times in FcHT-AuNPs. Scan rate: 50 mV/s. [FcHT-AuNPs] = 2.8 µM.

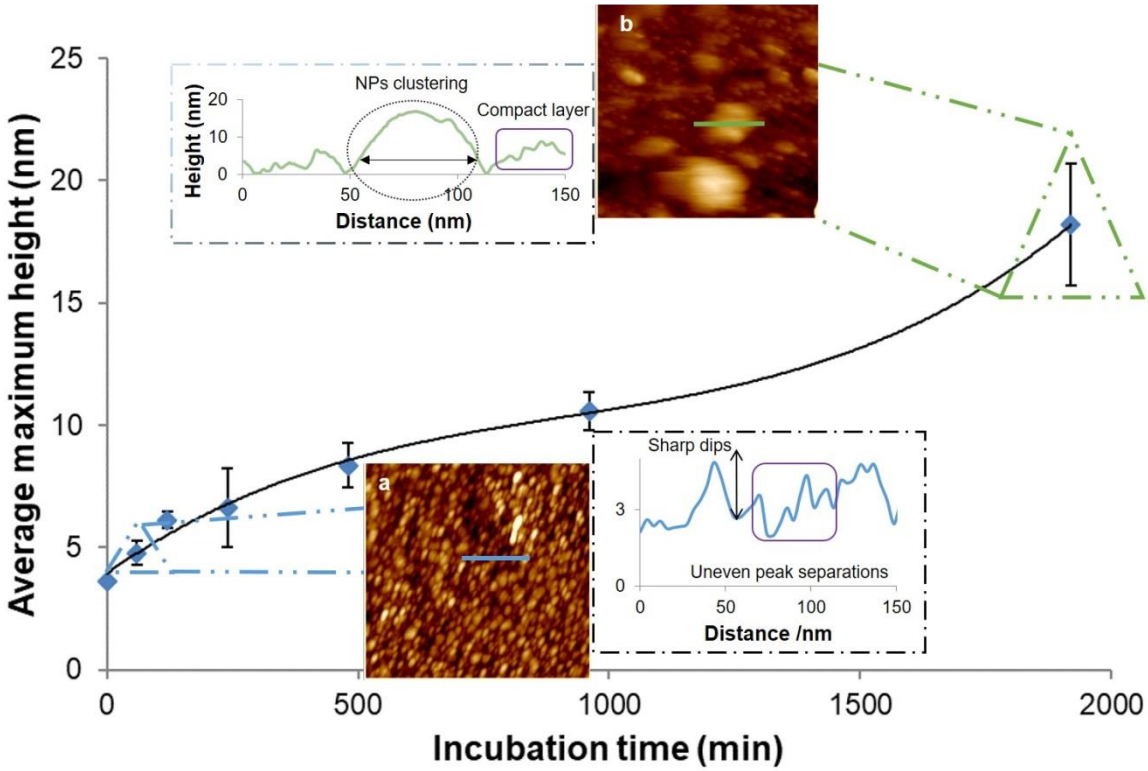

Figure 3: Time-lapsed study for the incubation of lipid immobilised substrates with DDT-AuNPs;
average max. height of NPs on the lipid surface at different incubation times with the NPs including
AFM images (a) after 60 min and (b) after 1920 min incubation in NPs solution. All images are 200 x 200 nm. [DDT-AuNPs] = 1.2 nM.

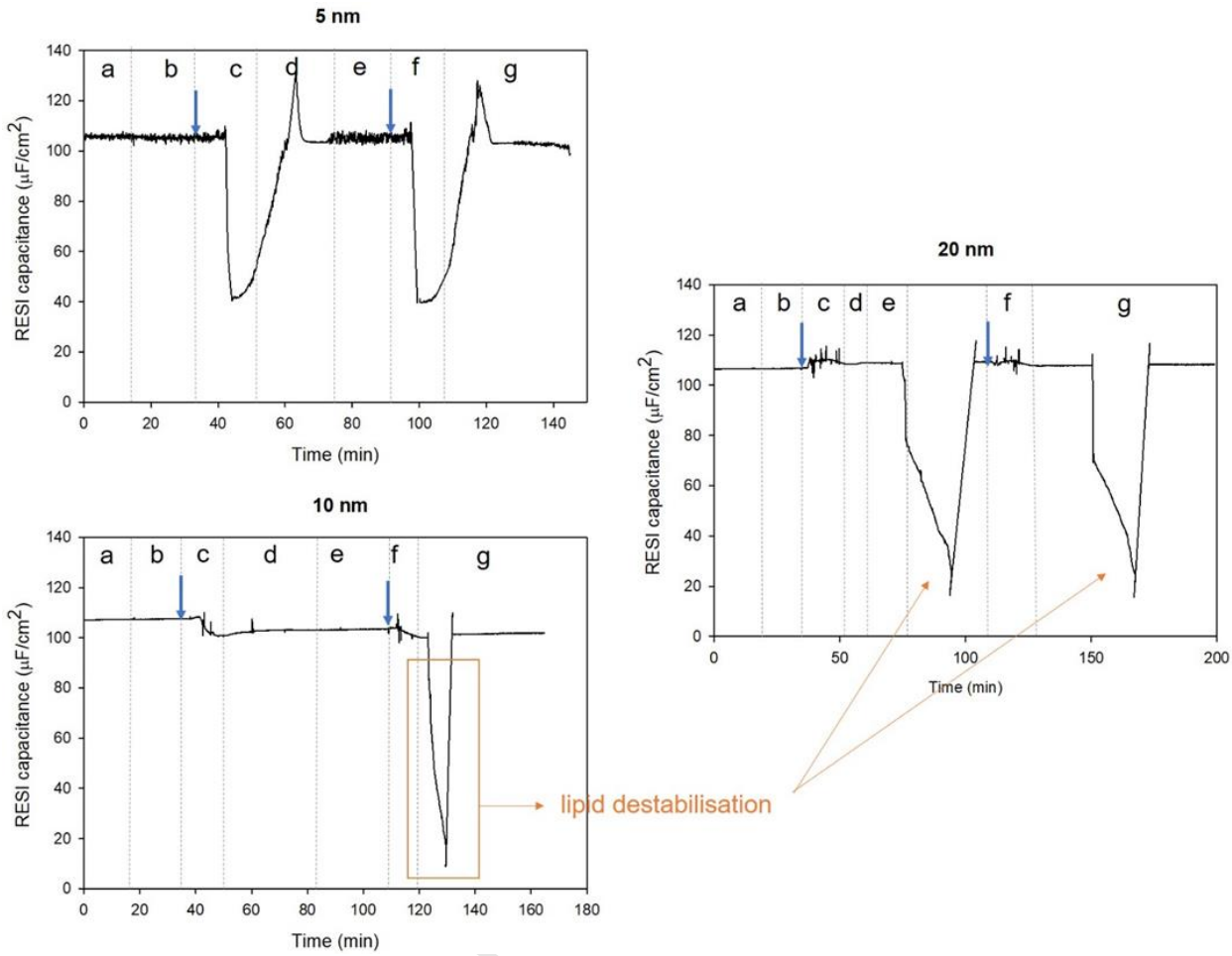

Figure 4: Change in RESI capacitance with FcHT-AuNPs injection over time as a function of NPs sizes; 5, 10 and 20 nm, a running electrolyte solution of 20 mM PBS at a set flow rate of 5 µL/min; the arrows representing the injection of NPs in the system. [5 nm FcHT-AuNPs] = 2.8 µM, [10 nm FcHT-AuNPs] = 3.0 µM and [20 nm FcHT-AuNPs] = 3.0 µM.
The key to alphabets used in the figures are:

(a) the stabilisation of the system for approximately 15 min at set flow rate of 5 µL/min with a constant flow of buffer (20 mM PBS). (b) = the injection of fresh solvent (deionised water) followed by 10 min of stabilisation. Stage (c) = the injection of 200 µl of AuNPs, dispersed in deionised water at a concentration of 200 nM into the system fitted with tBLM-modified gold sensors. Followed by a repeat of the earlier stages; buffer, solvent, NPs injection and buffer, for (d), (e), (f) and (g) respectively

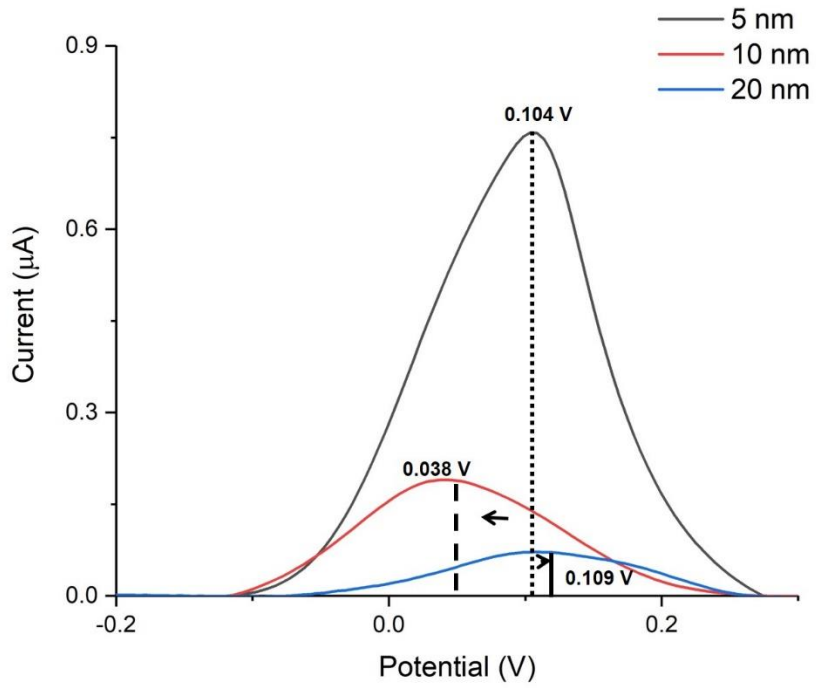

Figure 5: DPV responses of the penetration of FcHT-AuNPs (5, 10 and 20 nm) into tBLM-modified gold electrode (0.02 cm^2) in 20 mM PBS as a function of NP sizes. Sweep amplitude: 5 mV. [5 nm FcHT-AuNPs] = 2.8 µM, [10 nm FcHT-AuNPs] = 3.0 µM and [20 nm FcHT-AuNPs] = 3.0 µM.

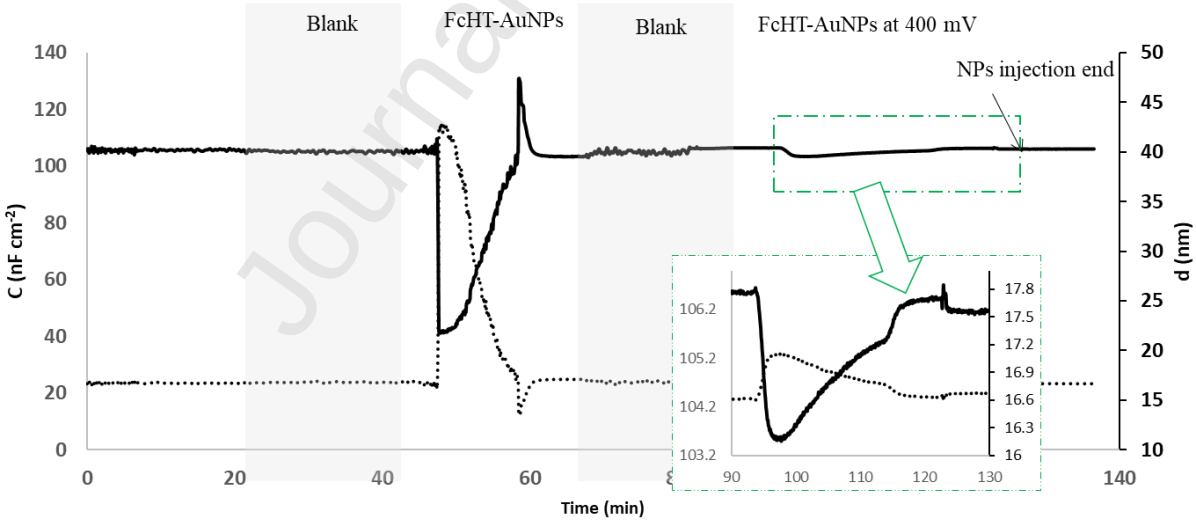

Figure 6: Change in RESI capacitance with FcHT-AuNPs injection over time as a function of potential controlled penetration through tBLM models on gold sensors; a running electrolyte solution of 20 mM PBS at a set flow rate of 5 µL/min.

Tables

Table 1: Electrochemical parameters determined by by DPV (ESI Figure S7) for the penetration FcHT-AuNP through SAM lipid membrane immobilised electrodes at different incubation times. Ip (optimised peak height), FWHM (Full Width at Half Maximum), Γ_t (Total reactants at the SAM modified electrode surface)
Q values calculated using CVs in Figure 2 are included in column 2

Incubation time (min)	**Q/ µC cm^{-2} (from CVs Fig 2)**	**Ip/A (from DPVs Fig ESI S7)**	**FWHM/mV (from DPVs Fig ESI S7)**	**Γ_T /mol cm^{-2} (Equation 1)**
60	32.1±5.3	2.2E-06	0.11	2.04 ± 0.20 E-10
120	40.2±4.3	2.1E-06	0.11	2.04 ± 0.65 E-10
240	28.2±4.8	1.68E-06	0.12	1.63± 0.76 E-10
480	33.5±3.5	3.56E-07	0.15	3.46±0.53 E-11
960	14.0±4.7	4.72E-07	0.16	4.59±0.24 E-11
1800	10.9±3.5	4.15E-07	0.18	4.03 ±0.59E-11

Table 2: Electrochemical parameters determined by DPV (Figure 5) for the FcHT-AuNP through tBLM lipid membrane immobilised electrodes for different NP sizes.

NPs size	**I_p/A**	**Γ_T/mol cm^{-2}**
5 nm	7.6E-07	7.38± 0.22 E-11
10 nm	1.9E-07	1.85±0.28E-11
20 nm	7E-08	6.80± 0.23 E-12

Credit Author Statement

Ritu Kataky: Conceptualization, Methodology, supervision, revision, editing

Yousilliya Bunga.: Laboratory work,- Original draft preparation#, Reviewing and Editing,

Declaration of interests

☒ The authors declare that they have no known competing financial interests or personal relationships that could have appeared to influence the work reported in this paper.

☐The authors declare the following financial interests/personal relationships which may be considered as potential competing interests:

Highlights

1. Resonance Enhanced Surface Impedance spectroscopy (RESI) senses nanoparticles (NP)
2. RESI enables real time measurements of NP-lipid layer interactions
3. Effects of NP size showed NPs >5 nm caused reversible lipid bilayer disruption.
4. NP incubation time, studied show agglomeration of NPs on electrode surface